



CHORUS

This is the accepted manuscript made available via CHORUS. The article has been published as:

Resonant interactions between discrete phonons in quinhydrone driven by nonlinear electron-phonon coupling

Aaron S. Rury

Phys. Rev. B **93**, 214307 — Published 24 June 2016

DOI: [10.1103/PhysRevB.93.214307](https://doi.org/10.1103/PhysRevB.93.214307)

Resonant interactions between discrete phonons in quinhydrone driven by nonlinear electron-phonon coupling

Aaron S. Rury*

Department of Chemistry, University of Southern California, Los Angeles CA, 90089, USA

This study reports experimental, computational and theoretical evidence for a previously unobserved coherent phonon-phonon interaction in an organic solid that can be described by the application of Fano’s analysis to a case without the presence of a continuum. Using Raman spectroscopy of the hydrogen-bonded charge-transfer material quinhydrone, two peaks appear near 700 cm^{-1} we assign as phonons whose position and line shape asymmetry depend on the sample temperature and light scattering excitation energy. Density functional theory calculations find two nearly degenerate phonons possessing frequencies near the values found in experiment that share similar atomic motion out of the aromatic plane of electron donor and acceptor molecules of quinhydrone. Further analytical modeling of the steady-state light scattering process using the Peierls-Hubbard Hamiltonian and time-dependent perturbation theory motivates assignment of the physical origin of the asymmetric features of each peak’s line shape to an interaction between two discrete phonons via nonlinear electron-phonon coupling. In the context of analytical model results, characteristics of the experimental spectra upon 2.33 eV excitation of the Raman scattering process are used to qualify the temperature dependence of the magnitude of this coupling in the valence band of quinhydrone. These results broaden the range of phonon-phonon interactions in materials in general while also highlighting the rich physics and fundamental attributes specific to organic solids that may determine their applicability in next generation electronics and photonics technologies.

I. INTRODUCTION

The spectrum of vibrational frequencies of a crystal’s lattice significantly impacts its thermodynamic properties and, therefore, its suitability in electronics and photonics applications¹. Typically, in order to calculate thermodynamic properties such as the heat capacity, one works in the harmonic limit in which a potential energy that scales with the negative square of the change in the position of atoms away from equilibrium dictates the frequency of a lattice vibration². However, the lattice vibrational frequencies of real crystals deviate from the harmonic limit. Phonon-phonon interactions represent one of the most important mechanisms by which this deviation occurs and can produce significant changes in the thermodynamic properties of materials³. Typically, one represents these interactions by expanding the potential energy experienced by the nuclei of a solid, V , in the normal coordinates of the crystal vibrations (Q_1, Q_2, \dots, Q_N) as,

$$V(Q_1, Q_2, \dots, Q_N) \approx V_0 + \sum_j \frac{1}{2} \frac{\partial^2 V(Q_j)}{\partial Q_j^2} \Big|_0 Q_j Q_k \quad (1) \\ + \sum_{j,k,l} \frac{1}{3!} \frac{\partial^3 V(Q_j, Q_k, Q_l)}{\partial Q_j \partial Q_k \partial Q_l} \Big|_0 Q_j Q_k Q_l + \dots,$$

where V_0 indicates the value of this potential energy at the equilibrium position of the nuclei, which we take at $Q_i = 0$. Explicitly, while the harmonic frequency of the j^{th} phonon vibration is set by the second term on the right side of Eq. (1), the higher order terms of this expansion represent the anharmonicity driven by phonon-phonon interactions. Given their importance in the behavior of nuclei in solids, understanding the physical

foundation of phonon-phonon interactions in candidates for next generation electronics and photonics technologies remains a necessity.

For many materials, neutron scattering and thermal transport measurements have been the experimental techniques of choice to investigate phonon-phonon interactions³. Neutron scattering allows connection between phonon anharmonicity and dispersion given the amount of momentum a neutron can transfer to the atoms in a solid sample. However, because these techniques interrogate phonons in steady-state electronic configurations, they lack the ability to capture phonon-phonon interactions in the presence of transient electronic densities. While typically only providing information on the transitions near the center of the Brillouin zone due to the conservation of linear momentum during the light scattering process, Raman spectroscopy has been used to uncover the complex nature of phonon-phonon interactions in technologically important inorganic materials ranging from bulk insulators⁴, including ferroelectrics⁵, to bulk semiconductors^{6,7} as well as organic graphitic materials⁸. Furthermore, by exciting the Raman scattering process with light whose energy matches that of transitions between electronic bands of a material, one can gain insight into the phonon-phonon interactions of transient electronic states not possible with neutron scattering and transport measurements⁹.

Previously, experimental evidence has predominantly pushed researchers to consider phonon-phonon interactions in Raman scattering spectra due to a physical mechanism similar to a Fermi resonance. That is, coupling between the fundamental excitation of a phonon, typically from the optical branch, with overtones and combinations of other phonons, either from the acoustic or optical branches, due to energy degeneracy.^{6-8,10} In this

physical picture of the Fermi resonance, the anharmonic behavior of phonons implied by the terms beyond the quadratic contribution to Eq. (1) can be described by perturbative corrections to a vibration’s self-energy due to the accidental degeneracy of the energy of the vibration of interest with that of overtone or combination bands. By examining Eq. (1), we see that these corrections begin to occur at the third order of perturbation theory, necessitating the interaction of at least three phonons. However, there is no *a priori* reason for the pre-dominance of this phonon-phonon interaction mechanism in all materials.

The natural abundance and solution processability of organic materials composed of electron donor and electron acceptor molecules, known as charge-transfer (CT) materials, make them desirable answers as sustainable technologies in electronics and photonics¹¹. In addition to the electronic properties of CT materials, researchers have added hydrogen-bonds for further functionality and found room temperature ferroelectric behavior¹² as well as coupled magnetic-electron transport effects¹³. In contrast to inorganic materials such as Si, Ge and ZnO that have been studied extensively using Raman scattering, the typically large number of atoms in unit cell of organic materials means that their phonon density of states can often be large. This increase of the density of phonon states relative to many simple inorganic materials seems to imply that one should anticipate stronger and new types of phonon-phonon interactions in organic materials with large numbers of atoms in their unit cell, especially in the presence of hydrogen bonding.

Quinhydrone is a hydrogen-bonded charge-transfer (HBCT) material formed from the co-crystallization of the electron donor hydroquinone (HQ) and the electron acceptor *p*-benzoquinone (BQ). This material was first discovered over 150 years ago and has long been used as an organic electrode¹⁴, but its basic physics have remained relatively unexplored. A visual representation of the unit cell with parameters found from x-ray diffraction is shown in Figure 1¹⁵.

The simplicity of quinhydrone makes it an accessible model material to understand the importance of lattice phonons in HBCT materials. The few previous studies undertaken on quinhydrone have already demonstrated how phonons drive interesting behavior in this material. Upon applying pressure along its *a*-axis, Mitani *et al.* found that the behavior of O-H stretching vibration of HQ changes dramatically and posited a cooperative proton-electron tunneling phase of quinhydrone that must be mediated by at least one lattice phonon¹⁶. Rury *et al.* have also shown that unlike other CT crystals, a Raman-active lattice phonon modulates electron transfer in the charge separated state of quinhydrone¹⁷. However, phonon-phonon interactions in quinhydrone and other HBCT materials remain totally unexplored territory thus far. Given the strong vibrational anharmonicity often found in hydrogen-bonded materials, quinhydrone provides a useful model for understanding the role

of phonon-phonon interactions in the presence of electron transfer where modeling of electron-phonon interactions is especially important¹⁸.

Electron-phonon coupling has been shown to be one of the most important attributes of low dimensional organic CT materials, leading to spin-Peierls distortions upon electronic excitation¹⁹, quantum para-electric phases²⁰ as well as other exotic phenomena²¹. Additionally, nonlinear electron-phonon coupling plays a role in the physics of two types of strongly correlated electronic phenomena. First, Cavatorta *et al.* have shown that the nonlinear contribution to electron-phonon interactions couples intra and intermolecular vibrations of the pseudo-1D CT material comprised of tetrathiafulvalene and chloranil upon the ultrafast photo-induced neutral-to-ionic transition of this material^{22,23}. Second, a wide array of both experimental and theoretical studies have shown that nonlinear electron-phonon coupling plays a central role in the anomalously high superconducting transition temperatures of MgB₂²⁴⁻²⁹. Therefore, finding other roles that electron-phonon coupling can play in determining the behavior of materials represents an important goal in the application of new physical phenomena in real world devices. Bozio and co-workers have shown that Raman spectroscopy can characterize electron-phonon coupling in organic CT materials, similar in their electron transfer interactions to quinhydrone^{30,31}.

Based on the pioneering work espousing both phonon-phonon and electron-phonon interactions in other materials using Raman spectroscopy, we have applied a combined experimental, computational and theoretical inelastic light scattering spectroscopic approach to uncover a previously unreported interaction between two of the phonons of the model HBCT material quinhydrone driven by electron-phonon interactions. Using single crystal, polarized Raman spectroscopy excited in resonance with separate electronic transitions of this material, we find two high frequency lattice phonons of quinhydrone whose behavior we explain with a mechanism similar to a Fano interaction, but without the need for a continuum of states. This behavior includes the mirrored behavior of the inverse of the asymmetry parameter and line width of each mode, which we show is in accord with Fano’s original treatment of the case of auto ionization in atoms and molecules. Furthermore, we find that this interaction depends on the energy used to excite the scattering process. Resonant excitation of electron transfer through an intramolecular transition of the electron acceptor of quinhydrone, BQ, enhances the interaction between the two modes and leads to increased asymmetry of the peak associated with each phonon relative to a near-IR resonant excitation of what we believe to be a excitonic electron transfer transition.

Ab initio electronic structure calculations of quinhydrone using density functional theory (DFT) find two nearly degenerate vibrations whose atomic motion is delocalized on both molecules of quinhydrone. These calculations provide evidence that the two phonons are com-

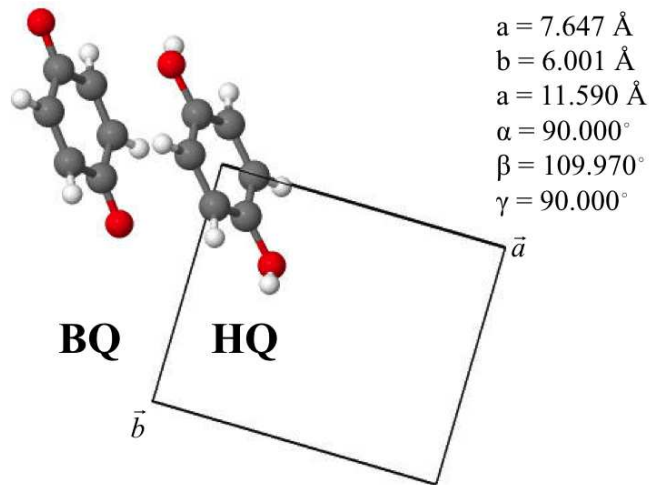


FIG. 1. (color online) Visual representation of the ab -plane of the crystallographic unit cell of monoclinic quinhydrone found from room temperature x-ray diffraction measurements¹⁵ showing the electron donor of the material, hydroquinone (HQ), on the right and the electron acceptor, p-benzoquinone (BQ), on the left. Lattice parameters are reported in the top right corner.

prised of nuclear motion out of the aromatic plane of each molecule. We propose that the frequencies and intensities of these modes become coupled due to their degeneracy and their ability to modulate electron transfer in quinhydrone. Based on this assignment of the modes and physical picture of the coupling mechanism, we analytically calculate model polaron wave functions in the presence of both first and second order perturbative corrections to adiabatic states due to electron-phonon coupling using a nonlinear Peierls-Hubbard Hamiltonian. We then use these polaron states to calculate Raman spectra using a first principles approach of time-dependent perturbation theory found by the interaction of these states with quantized incident and scattered electromagnetic waves. We find excellent agreement between the measured and calculated spectra that further motivates the assignment of a Fano-like resonant interaction between the modes under examination driven by electron transfer between the donor and acceptor sites of quinhydrone. Our data analysis and modeling also cast significant doubt on the alternative effects that may explain our results. Additionally, near-infrared excitation of a sample formed from the deuterated form of the electron donor of quinhydrone, hydroquinone (HQ), shows that the higher frequency of these two modes carries substantial motion of the hydroxyl hydrogen of HQ that has been previously proposed to dominate the proton transfer behavior of quinhydrone.

These experimental and theoretical results broaden the range of possible phonon-phonon interactions in solids as well as form a foundation on which further investigation of similar effects on other HBCT materials can be examined. In particular, doubts have been raised concern-

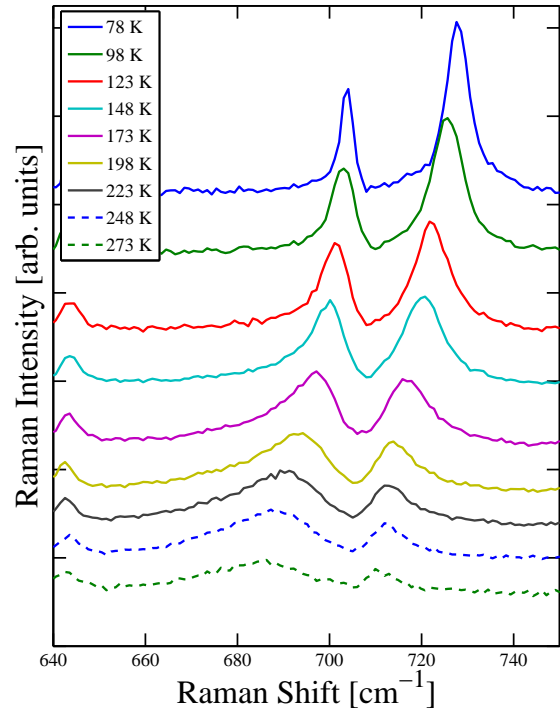


FIG. 2. (color online) Temperature dependent $z(xx)\bar{z}$ -polarized Raman scattering spectra of a monoclinic quinhydrone single crystal in the region between 640 cm^{-1} and 750 cm^{-1} excited at 2.33 eV .

ing the ability of specific hydrogen-bonded charge transfer materials to achieve room temperature ferroelectric phases, as reported by Tayi *et al.*. These doubts are based upon analytical results of the Peierls-Hubbard Hamiltonian when used in combination with computational inputs found from DFT calculations¹⁸. However, the results we find here provide evidence that higher order contributions to the Peierls-Hubbard Hamiltonian may be necessary to capture the relevant physics of HBCT materials. Therefore, for cases when electron transfer between donor and acceptor sites drives anharmonic coupling between phonons the results found in this study imply that Fano-like resonant interactions between vibrational states could play a meaningful role in the behavior of these materials and impact their application in electronics and photonics.

II. RESULTS

A. Experimental

Samples of monoclinic quinhydrone single crystals and temperature-dependent, polarized Raman spectra were formed and gathered in the same manner as described previously^{17,32}. Figure 2 shows the temperature-

dependent Raman scattering from a monoclinic quinhydrone single crystal in the region between 640 cm^{-1} and 750 cm^{-1} excited at 2.33 eV for the $z(xx)\bar{z}$ polarization configuration³³. We highlight to the reader that Rury *et al.* have shown that light at 2.33 eV likely excites an intramolecular electronic transition of BQ that drives intermolecular electron transfer in quinhydrone on time scales that could not be definitely determined with sub-100 fs resolution³². In the spectra of Figure 2, two peaks appear as broad, low intensity features at 273 K that shift in frequency, increase in intensity, and change in line width as we cool the crystal. We assign both features as phonons of quinhydrone. Given the previous notation of the Raman-active lattice phonons of monoclinic quinhydrone¹⁷, we denote the lower and higher frequency peaks as ν_6 and ν_7 , respectively.

Upon closer examination of Figure 2, one sees that both temperature-dependent peaks possess asymmetric line shapes, but in different directions of energy. The lower frequency of the two features has a fatter tail toward lower energy while we find the opposite case for the higher frequency peak. We also note that the asymmetry of each peak changes as a function of temperature. In addition, the scattering intensity at frequencies between these two peaks drops to zero. Furthermore, as shown in Figure 3, upon excitation of the same quinhydrone single crystal at 1.58 eV both the ν_6 and ν_7 modes appear, albeit with differences that will be discussed in detail below. The reader should note that while the spectra of Figure 2 are shown on a linear-linear scale, those of Figure 3 are shown on a linear- \log_{10} scale due to the dramatic increase in the intensity of Raman scattering excited at 1.58 eV caused by an increased ground state electron transfer upon cooling monoclinic quinhydrone³².

The temperature-dependent evolution of the line shapes of the two phonons becomes more interesting upon isotopic substitution of one of the oxygen-bound hydrogen atoms of HQ with deuterium. Figure 4 compares Raman spectrum of a 78 K monoclinic crystal of d_5 -quinhydrone excited at 1.58 eV to the spectrum scattered by a fully hydrogenated crystal at the same temperature. Two features stand out in this comparison. First, while ν_6 remains a single peak, ν_7 has become two peaks. Second, while the position of ν_6 remains approximately the same in the deuterated sample, the position of the ν_7 mode shifts to higher frequency, even when accounting for the doublet structure.

To understand the evolution of the line shape of the ν_6 and ν_7 modes upon cooling the quinhydrone crystal, we fit their line shapes using a Fano profile³⁴, as done previously by Cooper and co-workers^{35,36}. We use the equation,

$$I(\omega) = I_0 \frac{\left(q + \frac{\omega - \omega_0}{\Gamma_{eff}}\right)^2}{1 + \left(\frac{\omega - \omega_0}{\Gamma_{eff}}\right)^2}. \quad (2)$$

where ω_0 is the phonon frequency, Γ_{eff} is its effective line

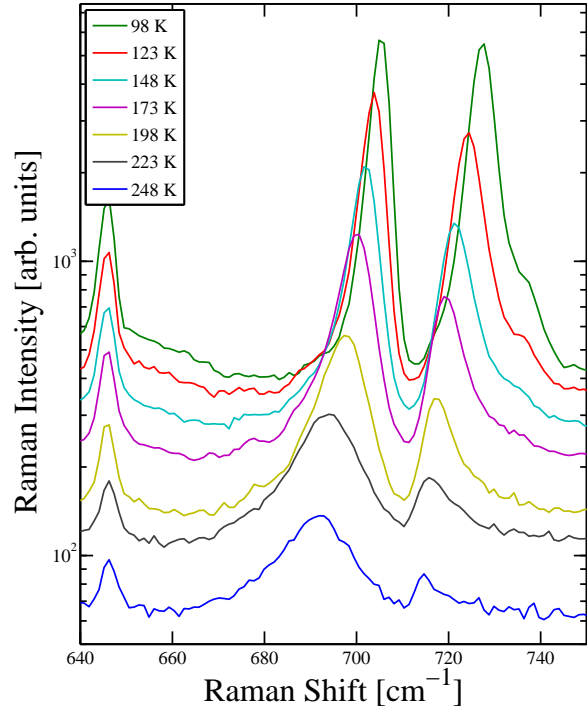


FIG. 3. (color online) Temperature-dependent, $z(xx)\bar{z}$ -polarized resonance Raman spectra of a monoclinic quinhydrone single crystal for excitation at 1.58 eV in the window of 640 cm^{-1} to 750 cm^{-1} shown on a linear- \log_{10} scale

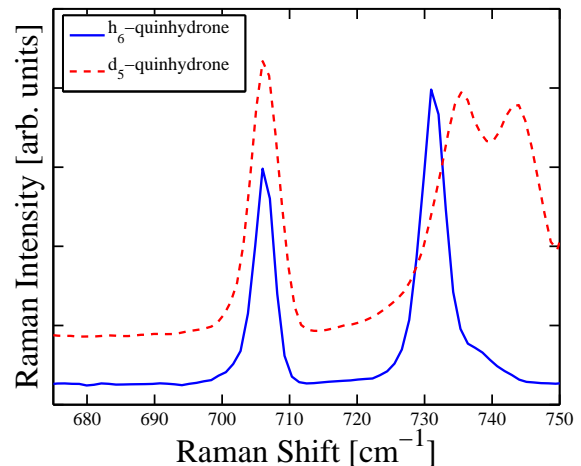


FIG. 4. (color online) Comparison of the Raman spectrum of fully hydrogenated single monoclinic quinhydrone crystal excited at 1.58 eV (solid) to the spectrum of a deuterated single monoclinic quinhydrone crystal excited at the same energy (dashed).

width and q is the asymmetry parameter, as defined by Fano. Figure S1 of the Supplemental Material (SM) compares the ν_6 mode in Figure 2 to fits using Eq. (2). Fits of the ν_7 mode in Figure 2 to Eq. (2) show similar agreement. In contrast, Figure S2 of the SM shows poorer fits of ν_6 to Eq. (2) for 1.58 eV excitation, especially at the lower temperatures used in our measurements. All parameters of the fits to Eq. (2) of the ν_6 and ν_7 modes at each temperature, including their associated uncertainty, for 2.33 eV excitation are found in Tables S1 and S2, respectively, of the SM. In the case of 1.58 eV excitation, the shoulder to the high energy side of ν_7 precluded its fit to Eq. (2) so that Table S3 only reports the parameters of the fits to Eq. (2) for the ν_6 upon near-IR excitation. Possible reasons explaining the presence of this shoulder and its effect on the interpretation of our results are discussed in Section III. To analyze the position of the ν_7 mode as a function of temperature the frequency of the peak intensity is taken, which can be extracted for all the temperatures except 273 K under our experimental conditions. Figure S3 of the SM shows that q for the ν_6 is smaller upon excitation at 2.33 eV relative to 1.58 eV for all temperatures considered in our study, even considering the error of the fits of the spectra to Eq. (2). This difference in the magnitude of q for each excitation laser implies that any interaction between the ν_6 and another resonance is larger upon 2.33 eV excitation than in the case of 1.58 eV.

The fits of the measured spectra to Eq. (2) allow one to compare the trends in peak position and frequency difference of the two modes as functions of temperature. The top panel of Figure 5 shows the temperature dependence of the position of each mode for each excitation energy. We find that simplest interpretation of these data is that the position of the higher frequency of these two peaks shifts linearly with temperature, while the lower frequency of the pair seems to asymptotically approach its frequency at low temperatures for both excitation energies. In addition, the frequency separation between the two features at each temperature changes as a function of excitation energy, as shown in the bottom panel of Figure 5. For 2.33 eV excitation, a larger frequency separates the two peaks than upon 1.58 eV excitation. The overall temperature dependence of the frequency difference is similar for each excitation energy. The behavior of the temperature dependence of the frequency difference between these two phonon modes seems largely dependent on the nonlinear trend in the ν_6 mode frequency. Since one would anticipate a linear dependence of a phonon frequency on temperature stemming from changes to the real part of the phonon's self-energy as explained previously^{6,7,37}, the nonlinear dependence of the peak position of the ν_6 mode for both excitation energies implies a separate mechanism must explain the change in its frequency as the temperature changes. The mechanism we believe leads to this temperature dependence is developed theoretically in Section II.C. and discussed in Section III.

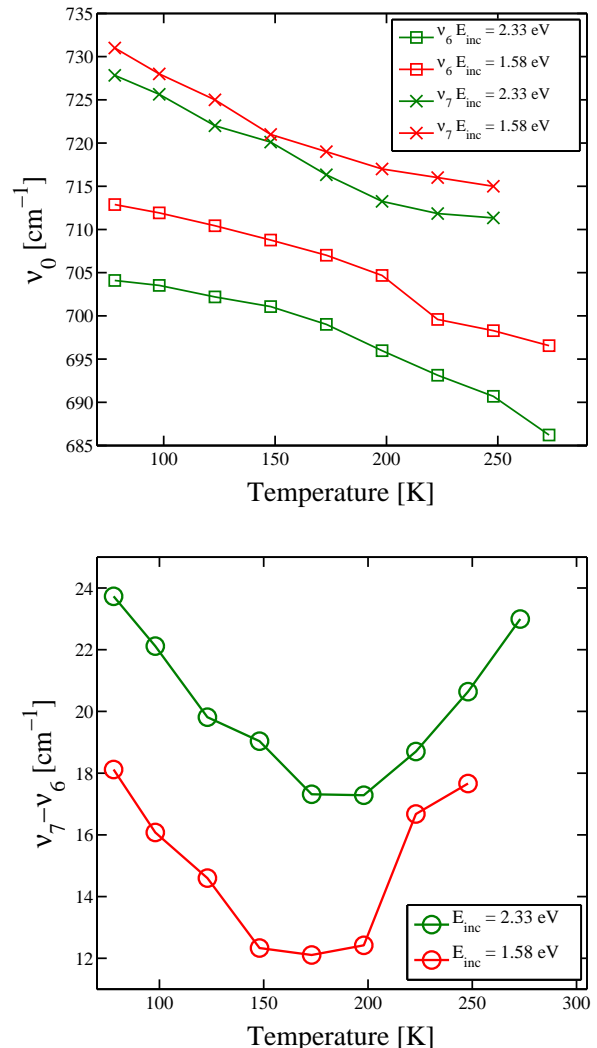


FIG. 5. (color online) Top: Comparison of the temperature dependence of the ν_6 (squares) and ν_7 (crosses) upon on excitation of a single monoclinic crystal of quinyhdron at 2.33 eV (green) to that for 1.58 eV excitation (red). Bottom: Comparison of the temperature dependence of the frequency difference of the ν_7 and ν_6 modes of monoclinic quinyhdron upon 2.33 eV (green) and 1.58 eV (red) excitation.

In Fano's seminal treatment, he showed that the line width of a measured peak can provide evidence of the presence of a resonant interaction between modes. Explicitly in the context of auto ionization, Fano stated 'This result shows that the configuration interaction "dilutes" the discrete state ϕ throughout a band of actual stationary states whose profile is represented by a resonance curve with a half-width $\pi|V_E|^2$. If the system under consideration were prepared in the state ϕ at a certain instant, it would auto ionize with a mean life $\hbar/2\pi|V_E|^2$ '.³⁴, where he had defined V_E as the interaction energy between a discrete state and a continuum. This statement means that the introduction of an interaction between

the state ϕ and a continuum results in a 'new' channel from which ϕ can decay, resulting in a line shape dominated by the interaction. While our case is physically distinct from that of auto ionization since there is no evidence of a continuum of any kind in our measurement, we believe that the spirit of Fano's statement appears in our spectra.

In Eq. (2), the asymmetry parameter, q , relates to the interaction potential between the resonances of interest via an inverse relationship, i.e. $V_{int} \propto \frac{1}{q}$. Therefore, by plotting the inverse of q as a function of temperature for each mode, we can determine how a would-be interaction between the two modes varies with this constraint. Comparison of the inverse of the asymmetry parameter with the line width at different temperatures then could provide insight into any coupling between these modes. The top panel of Figure 6 shows the temperature dependence of the line width (Γ_{eff}) extracted from fits of the measured spectra to Eq. (2) for the ν_6 and ν_7 modes of monoclinic quinhydrone measured upon excitation at 2.33 eV, while the bottom panel shows the temperature dependence of the magnitude of inverse of the asymmetry parameter, $|1/q|$ for the same excitation energy. These figures shows that line width and $|1/q|$ for each mode mirror each other in an interesting way. In the case of Γ_{eff} , we see that upon cooling the quinhydrone crystal the line width of ν_6 starts out at its largest value and then decreases, which is almost the exact trend shown by $|1/q|$ for the ν_7 mode. This trend can almost be read directly from the spectra shown in Figure 2 where the line shape of ν_7 closely resembles that of a Lorentzian below 123 K, which should be the case when $|1/q| \approx 0$. Similarly to the mirroring of Γ_{eff} for ν_6 and $|1/q|$ for ν_7 , the line width of ν_7 initially increases when cooled below 273 K until it reaches a maximum around 150 K and then decreases again, showing a striking similarity to the temperature dependent trend of $|1/q|$ for the ν_6 mode. It should be pointed out again that each peak in Figure 2 has been fit to Eq. (2) independent of the other such that there is no interplay between the parameters used to minimize the difference between the fit and data in the nonlinear least-squares algorithm we have used to find the parameters of Tables S1 and S2.

Fano's statement from his original work highlighted above provides an avenue to interpret both panels of Figure 6. When the interaction is strong between the modes, excitation of one mode, say ν_7 , will lead to more rapid transfer of the excitation to the coupled mode, ν_6 . Therefore in the presence of coupling, a large value of $|1/q|$ for ν_7 implies a large value of Γ_{eff} for ν_6 . In the opposite extreme, when the interaction is small for one mode, then one would anticipate that line width of the other mode would be small, indicating a smaller probability that the excitation decays from its original state. The panels of Figure 6 show that the ν_6 and ν_7 modes of quinhydrone display behavior consistent with this physical picture of a resonant phonon-phonon interaction. To our knowledge this is the first observation of this behavior in the pa-

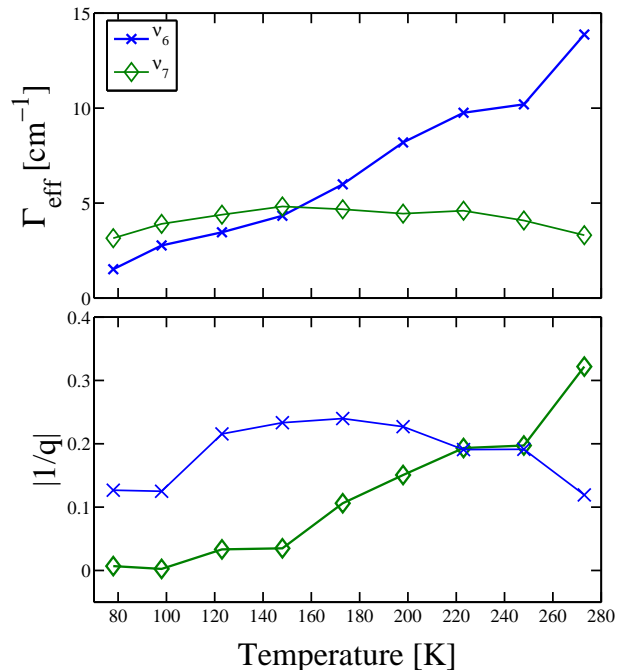


FIG. 6. (color online) Top: Comparison of the effective line width (Γ_{eff}) found for the ν_6 mode (crosses) to that of ν_7 mode (diamonds) of monoclinic quinhydrone extracted from fits of measured spectra excited at 2.33 eV to Eq. (2). Bottom: Comparison of the temperature dependence of the inverse of the asymmetry parameter, q , found from the same fits of the ν_6 mode (crosses) to that of ν_7 mode (diamonds) to Eq. (2) upon excitation of a single monoclinic crystal of quinhydrone at 2.33 eV.

rameters that define the dynamics of discrete vibrational excitations in a solid.

Despite the qualitative agreement in the temperature dependence of the line width and asymmetry parameter of each respective mode, inferring quantitative relationships between these parameters from the data shown in Figure 6 is difficult at this stage. This difficulty arises from the fact that while the resonant interaction between the ν_6 and ν_7 modes of monoclinic quinhydrone may be significant at the temperatures examined in Figures 2 and 3, other effects can also determine the decay channels of a given vibrational excitation of a crystal's lattice. Specifically in the case of this study, the top panel of Figure 6 shows that while the inverse of the asymmetry parameter of ν_7 plateaus very close to 0 for temperatures below 123 K, the line width of ν_6 continues to decrease when the crystal is further cooled. This change in the line width without a clear identification of the role of the interaction between the two modes along that decay channel shows that the temperature dependence of the compressibility of quinhydrone can still affect the self-energy of this vibration, as is expected of crystalline lattice phonons⁷.

Therefore, further study of quinhydrone that allows determination of the contribution from other effects that control the dynamics of vibrational excitations is necessary before a quantitative correspondence between Γ_{eff} and $|1/q|$ can be established.

While this treatment in the spirit of Fano motivates the physical picture that the ν_6 and ν_7 modes of monoclinic quinhydrone couple in a way unseen previously, this treatment provides no insight into the physical mechanism that leads to the interaction necessary to establish such a coupled system of vibrations. In order to establish this mechanism, we have undertaken both computational and analytical calculations to understand the types of vibrations likely involved in this interaction as well as its fundamental physics and their manifestation in Raman scattering spectra.

B. Computational

To assign the atomic motion corresponding to the ν_6 and ν_7 modes, we undertook *ab initio* electronic structure calculations using DFT. We use the Becke 1988 exchange functional³⁸ in combination with the Perdew-Wang generalized gradient approximation correlation functional³⁹, denoted as B3PW. These calculations use polarizable electronic basis sets for hydrogen⁴⁰, carbon⁴⁰ and oxygen⁴¹ atoms as implemented in CRYSTAL14⁴². This software package applies Bloch's theorem in conjunction with the symmetry operations of the space group of monoclinic quinhydrone to calculate its electronic bands. The positions of the atoms of monoclinic quinhydrone were set to those found in the room temperature x-ray diffraction pattern, reported previously¹⁵. The irreducible Brillouin zone of quinhydrone was set on a mesh according to Pack-Monkhorst sampling using a shrinking factor of 8 for all three crystallographic directions. Both IR and Raman-active vibrational frequencies of quinhydrone were found via the Coupled Perturbed/Kohn-Sham (CHKS) algorithm^{43,44}. This algorithm directly calculates the dipole, polarizability and hyper-polarizability using perturbation theory in response to an electric field applied to the different axes of the crystal of interest.

Upon completion of the DFT and CHKS calculations, we find two vibrations near 710 cm^{-1} whose atomic motions are not localized on either HQ or BQ. This fact gives us physical motivation to assign them as phonons whose frequency should change as a function of the thermally driven contraction of the crystal. We find both modes within 0.1 cm^{-1} of 713 cm^{-1} , but of different activity. The lower frequency of these two modes is A_g symmetry and Raman-active while the higher is A_u symmetry and IR-active. Vectorial representations of the lower and higher frequency of these two modes found from the calculation are shown in the left and right panels of Figure 7, respectively, as rendered by the software Jmol⁴⁵. In each panel of Figure 7, the electron acceptor, BQ, is shown on

the left and the electron donor, HQ, on the right and the white, gray and red sites correspond to hydrogen, carbon and oxygen atoms, respectively. Given their positions in frequency relative to the experimentally determined peak positions shown in Figures 2 and 3, we assign these two modes as ν_6 and ν_7 , although it's not clear which calculated vibration corresponds to which mode in the experiment. This assignment is made in Section III. It seems that by coupling the motion of these two intramolecular vibrations in a specific way, two new intermolecular phonons appear in the spectrum of quinhydrone unlike those of any reported organic charge-transfer materials previously. To identify the mechanism that can lead to this coupling, we turn to first principles analytical theory of the polaronic properties and light scattering spectra of charge transfer materials.

C. Theoretical

While the computational results in the previous section allow one to visualize the types of nuclear motion that likely correspond to the ν_6 and ν_7 phonon modes of quinhydrone, DFT calculations cannot alone determine the mechanism that would lead these vibrations to couple in a manner that results in the temperature dependent Raman scattering shown in Figures 2 and 3. In order to identify this mechanism, we calculated model Raman spectra from the second order correction in time dependent perturbation theory caused by the harmonic time varying incident laser and scattered electromagnetic fields in the presence of first and second order electron-phonon coupling.

The calculation of the Raman spectra begins with identifying the pertinent model Hamiltonian for the case of each excitation laser. Previously, Rury *et al.* used both resonance Raman and ultrafast transient reflectivity spectroscopies to show that intramolecular excitation of BQ in quinhydrone leads to electron transfer between the donor and acceptor of this material on time scales less than 100 fs ³². However, this conclusion relied on electron-phonon coupling manifest in the Raman scattering of the low frequency lattice phonons that differed substantially for visible and near-IR excitation. Therefore, one must take care in establishing the pertinent electronic Hamiltonian and basis states that can model the electron-phonon coupling in the case of each excitation laser. We believe that the Peierls-Hubbard Hamiltonian can handle the physics of both excitation processes, but since previous results more clearly identify a complete charge transfer excitation path for the 2.33 eV laser source, we focus our treatment here on this physical case.

Generally, we write the Peierls-Hubbard Hamiltonian of our model crystalline system as,

$$H_{tot} = H_e + H_{ph} + H_{e-ph}, \quad (3)$$

where H_e and H_{ph} correspond to the adiabatically separated contributions from the electronic, intermolecular

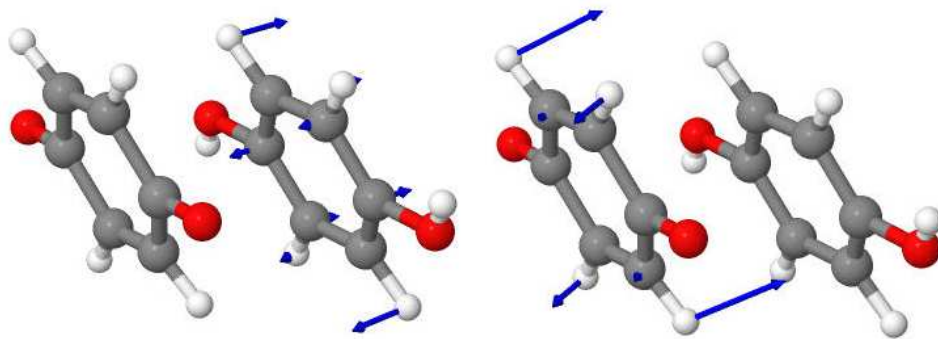


FIG. 7. (color online) Vectorial representation of the atomic motion of the A_g mode at 713 cm^{-1} (left pair) and the A_u mode at 713 cm^{-1} (right pair) found from DFT calculations using the B3PW global hybrid functional, as described in the text.

vibrational (ph) degrees of freedom of the charge transfer material, respectively. In addition, H_{e-ph} corresponds to the electron-phonon coupling contributions that we treat as perturbing the adiabatically separated Hamiltonian. H_{e-ph} in quinhydrone leads to new states created by mixing the eigenstates of both H_e and H_{ph} .

We use the Hubbard Hamiltonian for the electronic contribution to Eq. (3). In their second quantized form, the electronic and lattice phonon vibrational contributions to this Hamiltonian become,

$$H_e = \sum_{i,\sigma} \epsilon_i a_{i,\sigma}^\dagger a_{i,\sigma} + \sum_i U_i n_{i,\uparrow} n_{i,\downarrow} - t \sum_{i,\sigma} \left[a_{i,\sigma}^\dagger a_{i+1,\sigma} + a_{i+1,\sigma}^\dagger a_{i,\sigma} \right], \quad (4a)$$

$$H_{ph} = \sum_j \hbar \omega_j \left(b_j^\dagger b_j + \frac{1}{2} \right). \quad (4b)$$

The electronic Hamiltonian contains contributions from both the electron transfer integral t , the intra-site electron repulsion energy is U and $n_i = a_{i,\sigma}^\dagger a_{i,\sigma}$ is the electron number operator. The operator $a_{i,\sigma}^\dagger$ ($a_{i,\sigma}$) creates (annihilates) an electron on the i^{th} site in a spin state σ and the operator $n_{i,\uparrow}$ counts the number of electrons on i^{th} site with the spin state \uparrow . The operator b_j^\dagger (b_j) plays the same role as $a_{i,\sigma}^\dagger$ ($a_{i,\sigma}$), but in the case of the phonon with an energy $\hbar \omega_j$.

In general for molecular charge transfer materials like quinhydrone, there are two ways in which the vibrations contribute to the electron-phonon coupling Hamiltonian. First, lattice phonons of the material can modulate the transfer integral t , which creates the so-called nonlocal electron-phonon coupling⁴⁷. Second, intramolecular vibrations of the donor and acceptor molecules can modulate the on-site energy, ϵ_i , which leads to electron-molecular vibrational coupling^{46,48} or local electron-phonon coupling. Given the substantial out of plane atomic motion found from DFT calculations consistent with the frequencies of the peaks in our measurements, these modes should mainly modulate t . Therefore, we do

not treat local electron-phonon coupling in the present study. Inspired by the treatment of Bozio and co-workers^{30,31}, the electronic Hamiltonian, H_e , can be expanded in the N lattice normal coordinates, Q_j about their equilibrium position ($Q_j = 0$) as,

$$H_e(Q_1, Q_2, \dots, Q_N) \approx H_e(0) + \sum_j \left. \frac{\partial H_e}{\partial Q_j} \right|_0 Q_j + \sum_{j,k} \left. \frac{1}{2} \frac{\partial^2 H_e}{\partial Q_j \partial Q_k} \right|_0 Q_j Q_k + \dots \quad (5)$$

Eq. (5) shows that the single partial derivative of H_e with respect to the lattice normal coordinates gives the lowest order correction to electronic Hamiltonian due to electron-phonon coupling caused by electron transfer between sites. Using the standard relations between the coordinates of quantum harmonic oscillators and their associated creation and annihilation operators, this term takes the second quantized form,

$$H_{e-ph}^{(1)} = \sum_{i,\sigma,j} \left\{ g_j(\vec{k}_j) b_j^\dagger + g_j^*(\vec{k}_j) b_j \right\} \times [a_{i,\sigma}^\dagger a_{i+1,\sigma} + a_{i+1,\sigma}^\dagger a_{i,\sigma}]. \quad (6)$$

In Eq. (6), $g_j(\vec{k}_j)$ is the electron-phonon coupling constant that determines the strength with which the electron transfer process scatters a phonon of energy $\hbar \omega_j$ and depends on the phonon wave vector, \vec{k}_j . One can also think of this constant as the ability of a given phonon to modulate the electron transfer integral, t , of Eq. (4a). We refer to the inclusion of Eq. (6) in treating quinhydrone as *linear electron-phonon coupling*.

In addition to this lowest order contribution in Eq. (5), there is a second order contribution stemming from the expansion H_e in the lattice normal coordinates. In terms of the phonon creation and annihilation operators, this

term can be written as,

$$H_{e-ph}^{(2)} = \sum_{i,\sigma,j,l} \left\{ G_{jl}^{(1)}(\vec{k}_j, \vec{k}_l) b_j^\dagger b_l^\dagger \right. \quad (7)$$

$$+ G_{jl}^{(2)}(\vec{k}_j, \vec{k}_l) b_j^\dagger b_l + G_{jl}^{(3)}(\vec{k}_j, \vec{k}_l) b_j b_l^\dagger$$

$$\left. + G_{jl}^{(4)}(\vec{k}_j, \vec{k}_l) b_j b_l \right\} \left[a_{i,\sigma}^\dagger a_{i+1,\sigma} + a_{i+1,\sigma}^\dagger a_{i,\sigma} \right].$$

The terms $G_{jl}^{(m)}(\vec{k}_j, \vec{k}_l)$ determine the strength of each contribution to the second order e-ph coupling and depend on the wave vector of both phonon modes, j and l , in order to maintain the conservation of linear momentum in the crystal. Eq. (7) shows that in addition to the term proportional to $b_j^\dagger b_l^\dagger$ that excites overtones for $j = l$ and combination bands for $j \neq l$, there are two cross terms in the phonon creation and annihilation operators that also couple modes of different index in the case $j \neq l$. We refer to the inclusion of the second order corrections to the material Hamiltonian as *nonlinear electron-phonon coupling*. Since the spontaneous transfer of electron density from one site to the other that drives both linear and nonlinear electron-phonon coupling depends on the spacing of sites in the crystal lattice, these coupling constants should explicitly depend on temperature as dictated by the compressibility of the material of interest.

In the case of quinhydrone, theoretical assessments of the electronic structure of the HQ-BQ dimer in vacuum propose that this material is neutral in its ground state⁴⁹. Therefore, for a simple two site model we can first apply the results of Painelli and Girlando⁴⁶ to solve the Hamiltonians of Eqs. (4a) and (4b) followed by a calculation of the perturbations due to the first and second order e-ph coupling of the form of Eqs. (6) and (7). However, care must be taken in the choice of the electronic basis states used for the case of each excitation laser.

For the case of the 2.33 eV laser, the experimental evidence amassed thus far suggests that electron transfer from HQ to BQ is resonantly excited via an intramolecular transition of BQ. However, in the case of the 1.58 eV, previous experimental indications point to a distinct electronic state, which may be in excitonic in nature based on electron-phonon coupling interpreted from Raman spectra and the ultrafast dynamics probed in the near-IR region following visible excitation of quinhydrone single crystals³². While experiment⁵⁰ and theory⁵¹ suggest that electronic excitation of BQ in the region around 2.33 eV is a singlet-to-triplet $n \rightarrow \pi^*$ transition in the solid-state and gas phases, respectively, there is no evidence on the assignment of this transition in quinhydrone. Therefore, for simplicity we propose that one should use a basis set of states similar to those introduced by Painelli and Girlando⁴⁶. To determine the effect of nonlinear electron-phonon coupling, we use a natural basis set of electronic

states written as,

$$|\Phi\rangle = |\uparrow\downarrow, 00\rangle, \quad (8a)$$

$$|\psi_\pm\rangle = \frac{1}{\sqrt{2}} [|\uparrow 0, 0 \downarrow\rangle \pm |0 \downarrow, \uparrow 0\rangle], \quad (8b)$$

$$|\Theta_a\rangle = |0 \downarrow, \uparrow\downarrow, 0 \downarrow\rangle, \quad (8c)$$

$$|\Theta_b\rangle = |\uparrow 0, \uparrow 0\rangle, \quad (8d)$$

where the notation $|s_1 s_2, s_3 s_4\rangle$ is read from left to right as the pair of spin states of the electrons on the donor, HQ and then the pair of electron spins on BQ. In this context, the state $|\Phi\rangle$ corresponds to the localization of the electron density on the donor site of the model while the states $|\Psi_\pm\rangle$ and $|\Psi_\pm\rangle$ thru $|\Theta_{a,b}\rangle$ correspond to the singlet and triplet configurations of the charge-separated states of the two site mode, respectively. Diagonalizing the Hamiltonian of Eq. (4a) using the basis states in Eq. (8) hybridizes $|\Psi_+\rangle$ with $|\Phi\rangle$ giving two states that we denote as $|\Psi_A\rangle$ and $|\Psi_B\rangle$, written as

$$|\Psi_A\rangle = a_1 |\Phi\rangle + a_2 |\psi_+\rangle, \quad (9a)$$

$$|\Psi_B\rangle = a_2 |\Phi\rangle - a_1 |\psi_+\rangle. \quad (9b)$$

For the case of 2.33 eV excitation of electron transfer in quinhydrone, we can limit our treatment to $|\Psi_A\rangle$ and $|\Psi_B\rangle$. Given our assignment of an excitonic transition resonant at 1.58 eV, it is difficult to imagine the exact form of natural electronic basis sets one should use for that experimental situation. However, even given the possible many-body nature of this state, a similar electron-phonon coupling mechanism likely gives rise to our observations, as explained below. To understand the effects of both first and second order e-ph coupling we now only explicitly treat the states in Eq. (9) for the sake of simplicity and then motivate a physical picture for the case of 1.58 eV excitation that captures the necessary physics to explain our results.

To consider the role of electron-phonon coupling terms like that of Eqs. (6) and (7) in inelastic light scattering, we start with model adiabatic wave functions of the form $|\Psi\rangle|n\rangle_j|m\rangle_l$ for the j^{th} and l^{th} phonon eigenstates of H_{ph} where $|\Psi\rangle$ corresponds to one of the electronic eigenstates of H_e in Eq. (9). In the case where only the ground vibrational state of quasi-neutral ground electronic state, $|\Psi_A\rangle$, is populated (i.e. $n = m = 0$), we propose that the resonance Raman scattering from the j^{th} mode uses quantum paths containing the low lying phonon states of the participating excited electronic state: $|\Psi_A\rangle|0\rangle_j|0\rangle_k \rightarrow |\Psi_B\rangle|0\rangle_j|0\rangle_l \rightarrow |\Psi_A\rangle|1\rangle_j|0\rangle_l$ and $|\Psi_A\rangle|0\rangle_j|0\rangle_l \rightarrow |\Psi_B\rangle|1\rangle_j|0\rangle_l \rightarrow |\Psi_A\rangle|1\rangle_j|0\rangle_l$. Therefore, in order to correctly treat $H_{e-ph}^{(1)}$ and $H_{e-ph}^{(2)}$ we must apply do so for all of the states participating in the full light scattering process.

The full form of the wave functions resulting from perturbations due to linear and nonlinear electron-phonon coupling are shown in Appendix A. Eqs. (A1a)-(A4d) show that the excited vibrational state of the j^{th} mode

couples to the l^{th} mode in the final state of the scattering process, $|\Psi_2\rangle$, by introducing nonlinear e-ph coupling. The level of mixing is determined by the value of $G_{jl}^{(3)}$ for the modes of interest. Therefore, we can now see how the Peierls-Hubbard Hamiltonian including both first and second order e-ph coupling can lead to phonon mode mixing.

It is important to disentangle the physical meaning of the calculated wave functions in Eqs. (9) and (A1). Since there is a repulsive term in the Hubbard Hamiltonian denoted U that characterizes the Coulomb interaction between the electrons on a given site, there is a spontaneous tendency for the electronic density to delocalize between the two sites. In response to this spontaneous delocalization of the electrons between sites, the lattice must conserve any momentum created by exciting specific phonons. In the presence of an existing phonon excitation, nonlinear electron-phonon coupling dictates that a spontaneous transfer from one site to the other can then also transfer vibrational excitation from the normal modes of one phonon to those of a different phonon.

The fact that we have only considered a single Raman active mode, j , in deriving Eqs. (A1a)-(A1d) factors importantly into our interpretation of the measurements of Section II.A. This is because the DFT calculations of Section II.B found that one of the two degenerate vibrations at 713 cm^{-1} possesses A_u symmetry and is IR-active. However, the electron-phonon coupling Hamiltonians of Eqs. (6) and (7) show that in order to become active via this mechanism a given phonon mode only needs to modulate the electron transfer integral, t . Since the atomic motion of both of the modes shown in Figure 7 clearly change the orbital overlap of the donor and acceptor molecules, it seems reasonable that both of these modes can directly change the value of t . Thus, the linear and nonlinear electron-phonon coupling constants for the l^{th} mode, g_l , $G_{ll}^{(1)}$ and $G_{jl}^{(3)}$, should be non-zero for such a mode.

In the context of a possible excitonic state excited by 1.58 eV, Eqs. (A1) shows that in order for a similar mechanism to give rise phonon mode mixing, the excited state populated by an electronic transition resonant with light at this energy must use the lattice vibrations to couple to both the initial and final states participating in the Raman process. Even given the many-body nature of an excitonic state, if such a state carries substantial character from electron transfer between the donor and acceptor is not hard to see that any changes in t would directly affect the energy of this state and couple it to the ground state. Therefore, while we cannot realize an efficient way to express an excitonic state in terms of the electron spins on the donor and acceptor sites of a two site model in a manner similar to Eq. (8), excitonic electron transfer polaronic states of a similar form to Eqs. (A1) must characterize the effects of linear and nonlinear electron-phonon coupling on these states.

With the wave functions found from inclusion of both linear and nonlinear electron-phonon coupling, one can

proceed to determine the effects of these interactions on resonantly enhanced light scattering spectra. The full derivation of the second order time-dependent corrections due to the incident and scattering electromagnetic fields is found in Appendix B, where Eq. (B5) shows the explicit form of this corrections. Examination of Eq. (B5) shows that the line shapes of the j^{th} and l^{th} modes of a two-site model of quinhydrone get contributions from two different scattering pathways. While the first line of Eq. (B5) shows the Lorentzian line shape one expects from vibrational Raman peaks, the second line represents interference between the quantum paths participating in the scattering process caused by the resonant interaction of these two phonons driven by e-ph coupling, as has been described in detail previously for other physical circumstances⁵². Eqs. (B3a), (B3b) and (B4) show the parameters of the experiment that define the relative contribution from the terms of Eq. (B5). These include the linear and nonlinear electron-phonon coupling constant matrix elements with respect to states $|\Psi_A\rangle$ and $|\Psi_B\rangle$ as well as the detuning of the laser frequency, ω_L , from the frequency of the resonant electronic transition of choice, i.e. ω_{13} or ω_{14} . Therefore, using the temperature-dependent peak position, intensity and effective line width extracted from the fits of the measured spectra to Eq. (2), we can calculate the spectral shape of the Raman spectrum in the presence of linear and nonlinear electron-phonon coupling as one would expect from the expansion of the electronic Hamiltonian in the lattice phonon normal coordinates, as shown in Eq. (5).

Figure 8 compares the experimental spectra for temperatures of 78 K, 173 K, and 248 K to calculations using Eq. (B5) with the parameters in Tables S1 and S2 for the mode frequency (ω_j and ω_l) and mode line width (Γ_j and Γ_l) as well as the experimentally determined relative intensity of the two modes in the case of that A_j and A_l have opposite sign. Inspection of this comparison shows excellent agreement between our model and measurements. Interpretation of the using above treatment leads us to propose that nonlinear e-ph coupling between the ν_6 and ν_7 modes of monoclinic quinhydrone causes the interference between the scattering pathways of the Raman process, as seen in Eq. (B5), leading to a deviation from the harmonic frequency of each phonon mode and the asymmetric line shape of each peak. For the case of 2.33 eV excitation we also find ourselves in a fortunate situation. Unlike 1.58 eV excitation, no meaningful change is observed in the integrated intensity of any of the peaks below 650 cm^{-1} for 2.33 eV³². Based on this consideration, it seems reasonable to conclude that the energy of the transition excited by 2.33 eV does not change with temperature. Therefore, any change we see in the relative intensity of the two modes in our spectra should derive from changes in the other parameters driving the interactions, i.e. the linear and nonlinear electron-phonon coupling constants. To undertake this assessment of the contribution of each coupling constant, we must first identify a given peak in our spectra with

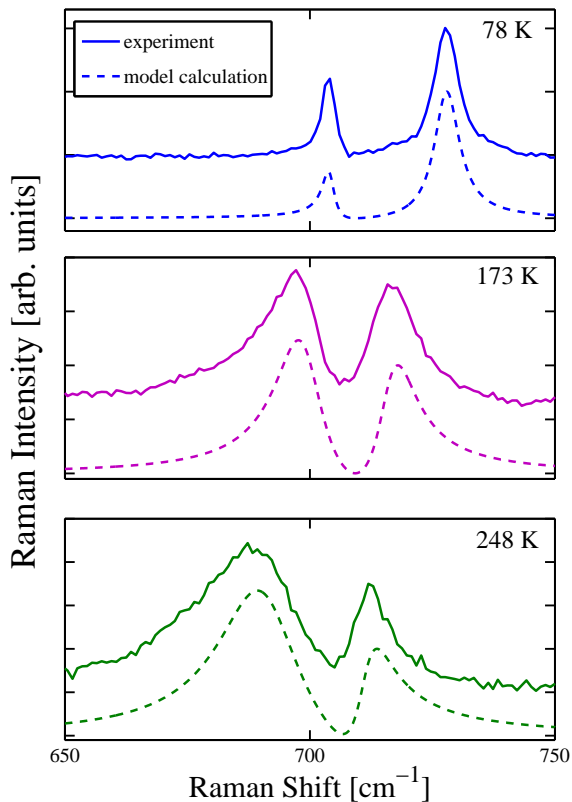


FIG. 8. (color online) Comparison of the experimental Raman scattering spectra of a single monoclinic crystal of quinhydrone excited at 2.33 eV (solid) to model spectra calculated from a first principles model based on nonlinear electron-phonon coupling(dashed) for temperatures of 78 K (top), 173 K (middle), and 248 K (bottom).

a specific mode in the model. This is achieved below in Section III, where we can assess the strength of these different interactions in the context of the other relevant attributes of our study as well as consider other possible explanations of our experimental results.

III. DISCUSSION

Results from experiment, computation and theory seem to support a hypothesis that the ν_6 and ν_7 modes of quinhydrone couple resonantly in a manner similar to a Fano resonance, but in the absence of a continuum. In particular, these modes possess line shapes of opposite asymmetry, DFT calculations find nearly degenerate delocalized vibrations of different irreducible representations near the experimentally determined frequencies, and a first principles time-dependent theoretical model of the light scattering process in the presence of linear and nonlinear electron-phonon interactions qualitatively reproduces our experimental results. Furthermore, the

characteristics of the experimentally determined temperature dependence of the line width and asymmetry parameter of these two modes mirror each other in manner qualitatively consistent with a Fano-like mechanism that couples these vibrations. However, these facets of our results do not conclusively prove the Fano-like resonant hypothesis and there remain three important attributes of the spectra whose explanation needs to be made within the context of our proposed mechanism.

One possible alternative explanation for the appearance of the line shape of each peak at each excitation energy is the simple linear combination of other peaks whose small intensity may not allow one to discern them as distinct features. In fact, Figure 3 shows that a small shoulder appears to the higher energy side of ν_7 at 98 K. However, when we consider all of the experimental evidence in the context of our technical capabilities, this possibility does not appear as a likely explanation of our experimental results for two reasons.

First, while Figure 3 shows a shoulder near 740 cm^{-1} at 98 K for 1.58 eV excitation, no such shoulder exists in the case of 2.33 eV excitation. In fact, the fits of the 78 K and 98 K spectra of the ν_7 mode upon 2.33 eV excitation shown in Figure 2 to Eq. (2) find that their line shapes are almost perfect Lorentzians, even when considering the region significantly higher in frequency than 740 cm^{-1} . Second, we point out once more that Figure 3 shows spectra on a linear-log₁₀ scale since the intensity of the light scattering excited at this energy changes so dramatically as the quinhydrone crystal cools. Therefore, the shoulder seen at 98 K is more than an order of magnitude lower than the peak of ν_7 . Also, we have reason to believe that the presence of this shoulder in the spectrum excited at 1.58 eV is largely technical. The commercial Raman spectrometer used in our measurements is designed for full polarization control of the incident and scattered light through computer-controlled optics inaccessible to the user in any other manner. Therefore, the user is limited by software in adjusting the exact rotation of wave plates and polarizers used to control the polarization of each light field.

While our control measurements have shown that this does not affect the results for 2.33 eV excitation, we find that measurements conducted at 1.58 eV deviate significantly from established polarization ratios for isotropic samples. Specifically, we tested the ability of the instrument to reproduce the reported depolarization ratio ($\rho = I_{\parallel\perp}/I_{\parallel\parallel}$) of the 992 cm^{-1} totally symmetric ring stretching vibration of benzene liquid, which Skinner and Nilsen found to be 0.02⁵³. While the experiments at 2.33 eV can achieve this previous result within 30%, those carried out at 1.58 eV produce a depolarization ratio almost a factor of 2 larger than 0.02. In addition, DFT calculations find a B_g vibration near the frequency of 715 cm^{-1} whose intensity is predicted to be significantly larger for the $z(xy)\bar{z}$ polarization configuration than the $z(xx)\bar{z}$ configuration. Therefore, a small change in the polarization fidelity of the incident electromagnetic field

could explain the presence of a shoulder on the order of a few percent the height of the main peak of interest. In addition, since all of our measurements suggest that each laser excites a separate electronic transition of quinhydrone, it becomes difficult to compare the behavior of the spectra between the different sources since some modes may appear for one laser and not the other.

An additional alternative explanation is the Fermi resonance mechanism thoroughly explained previously and examined in several other materials^{6,7,10}. However, when we consider the frequencies of the ν_6 and ν_7 modes, this mechanism also seems an unlikely explanation of our results. The ν_6 and ν_7 modes lie at energies more than twice as high as the other lattice phonons of quinhydrone and no other phonons appear in the spectral window of Figures 2 and 3. Therefore, in order to obey the energy conservation necessary for a Fermi resonance, overtones higher than second order would be required. However, there is no evidence for even the first overtone of any of the lattice phonons of monoclinic quinhydrone in our Raman spectra, making the possible excitation of higher order overtones very unlikely.

In addition to considering alternative explanations for the line shape of each peak in Figures 2 and 3, the model proposed in Section II.C. must account for the temperature dependence of three attributes of the experimental spectra highlighted above: the peak position of the ν_6 mode, the frequency difference between the two modes as a function of excitation laser energy, and relative intensity of each peak. As shown in Figure 5 of Section II.A., the peak position of the ν_6 mode shifts nonlinearly with temperature for both excitation lasers. This similarity in the temperature dependence of the mode position seems to imply that this behavior is associated with the valence band of quinhydrone. While one would anticipate a linear dependence of this peak, the treatment of electron-phonon coupling in Section II.C. shows that there is a mechanism for the deviation from this expectation: nonlinear electron-phonon coupling. In determining the perturbation to $|\Psi_A\rangle$, we found a term that uses the nonlinear e-ph coupling interaction Hamiltonian of Eq. (7) to mix $|\Psi_A\rangle$ with $|\Psi_B\rangle$ while creating no net excitations of lattice. Eq. (A1b) shows that the spontaneous transfer of an electron from donor to acceptor could cause the excitation of one lattice mode to transfer to another phonon of the lattice with a strength $G_{jl}^{(3)}$. In this way, one could equate this term with an anharmonic coupling between the j^{th} and l^{th} modes driven by electron transfer. Additionally, since this occurs for ν_6 in our data and would necessitate $G_{jl}^{(3)}$ theoretically, we can tentatively assign ν_6 as the l^{th} mode in our treatment of Section II.C. Given that this mode appears theoretically because of its coupling to the Raman-active j^{th} mode, it seems likely that ν_6 corresponds to the IR-active A_u mode found from DFT calculations.

Despite this tentative assignment, proving that nonlinear e-ph coupling leads to the exact temperature dependence of Figure 5 is significantly more complicated. In

order to quantitatively determine the temperature dependence of frequency and line width of a particular vibration one would anticipate from a two-mode anharmonicity driven by electron-phonon interactions, one would have calculate the effect of this anharmonic coupling on the phonon self-energy in a similar manner to the treatment of Crowley and others^{6,7,10}. While DFT calculations might allow us to grossly estimate the derivatives of the electronic Hamiltonian leading to e-ph coupling if we had access to the source code of the software used in this study, we simply do not have the other types of data on quinhydrone that would allow us to undertake any kind of meaningful numerical calculation to compare to our data. These data would include the temperature dependent lattice parameters of the crystal as well as the Grüneisen parameter for this material. Nonetheless, nonlinear e-ph coupling at least provides a plausible mechanism by which two-mode anharmonicity can affect the temperature dependent real part of the phonon self-energy and cause a nonlinear temperature dependence of the peak position.

While the effect of e-ph coupling on the valence band of quinhydrone likely explains the temperature dependence of the ν_6 , it is the effect of this coupling on the excited bands of quinhydrone that leads to difference in the frequency separation of the two modes of interest as a function of the laser excitation energy. The bottom panel of Figure 5 shows that difference in frequency between the ν_6 and ν_7 modes increases by almost 10 cm^{-1} for certain temperatures when we change the excitation laser from 1.58 eV to 2.33 eV. This change can be explained by the difference in the linear e-ph coupling constant, g_l , in the different states excited at each laser energy. Since the frequency of a given vibration depends explicitly on the electronic configuration, the frequency of a given vibration should depend on whether electron transfer becomes optically induced in the fully charge separated state versus a bound state like that of an exciton. Since most of the deviation in the difference between the two modes derives from the position of ν_6 , it seems that the coupling of this mode to electron transfer most sensitively determines its frequency in each of the respective excited bands probed in our measurements. Thus, the difference in the frequency of the ν_6 as a function of laser energy could serve as a probe of e-ph coupling in different electronic bands once definite assignment of these bands is established.

With tentative assignment of the ν_6 mode of quinhydrone as the l^{th} mode of our analytic model, we can begin to assess the strength of the electron-phonon coupling constants through the relative intensity of each peak in the measured spectra using the development of the calculated Raman spectra found from time-dependent perturbation theory. Eq. (B4) shows that the relative peak amplitude of the contribution of the j^{th} to that of the l^{th}

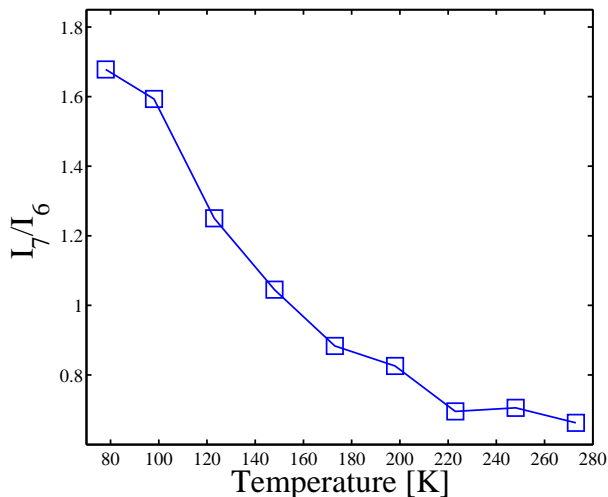


FIG. 9. (color online) Comparison of the experimental determined ratio of the peak intensity of the ν_7 mode to that of the ν_6 excited at 2.33 eV for temperatures between 78 K and 273 K.

mode is

$$R_A = \frac{A_j (\omega_{13} - \omega_L + i\Gamma_l)}{A_l (\omega_{14} - \omega_L + i\Gamma_j)}, \quad (10)$$

where A_j and A_l have been defined in Eq. (B3) and are proportional to the linear and nonlinear electron-phonon coupling constants, g and G , respectively. The square of Eq. (10) should be roughly proportional to the relative intensity of each peak in our spectra. When we compare Eq. (10) to the experimentally determined ratio of the ν_7 peak intensity to that of the ν_6 peak for each temperature for 2.33 eV excitation, an interesting trend appears. This ratio of the peak intensities is shown in Figure 9. In Figure 9, we see that while the peak intensity of the ν_6 mode is larger than that of ν_7 for temperatures above 173 K, the opposite holds for temperatures below 150 K. In fact, at 78 K, the intensity of ν_7 is almost a factor of 2 larger than ν_6 . This increase is even more significant when we consider the fact that Γ_l in the numerator of Eq. (10) corresponds to the line width of ν_6 , which decreases by an order of magnitude when the quinhydrone crystals cool from 273 K to 78 K. Since we pointed out above that there is no experimental evidence to support a change in the energy of the transition excited at 2.33 eV based on the integrated intensity of the other phonon peaks of quinhydrone, this temperature trend in Figure 9 must be driven changes in the model parameters expressed in Eqs. (B3a) and (B3b): g_j^* , g_l , G_{jj} , G_{ll} and G_{jl} . Broadly, the temperature trend in Figure 9 seems to indicate that the matrix elements in the basis of $|\Psi_A\rangle$ and $|\Psi_B\rangle$ of g_j^* , G_{jj} and/or G_{ll} either grow in strength as the crystal is cooled or those matrix elements of g_l and G_{jl} reduce in magnitude. In the context of the fits of the experimental spectra to Eq. (2) which show that the

$|1/q|$ for the ν_7 mode decreases in a manner similar to the increase in the relative intensity of Figure 9, it is likely that the trend in Figure 9 shows the decrease in G_{jl} as the sample cools. If this term represents the transfer of excitations of the ν_6 mode to ν_7 , then as it reduces we would expect to see an overall increase in the scattering intensity from the ν_7 , as shown in Figure 9. Thus, the temperature dependence of the relative intensities of the two peaks from our experimental data provides further evidence that the nonlinear electron-phonon interaction between two phonon modes drives the phenomena observed in this study.

As a final point of discussion, Figure 4 shows the change we observe upon the isotopic substitution of 5 of the hydrogens of HQ with deuterium. As pointed out in Section II.A., the ν_7 mode splits and becomes two modes of similar intensity, while the ν_6 mode remains relatively unchanged. The change in the appearance of the ν_7 mode seems to highlight a significantly larger contribution from hydroxyl hydrogen motion to this mode than to ν_6 and would be much more sensitive to hydrogen bonding in quinhydrone. This behavior of the ν_7 mode upon isotopic substitution further motivates our assignment of ν_6 as the non-Raman-active l^{th} mode of model since one would expect modes more localized on HQ to more sensitively change in response to the chemical substitution made in our measurements. However, the DFT calculations of Section II.B. show that this mode should be Raman-active. Therefore, ν_6 must be the IR-active mode, which corresponds to l in our model above.

The physical reason for the splitting is likely a symmetry breaking in the vibrational eigenstate due to the difference in the mass of hydrogen and deuterium. However, the fact that a Raman-active mode that carries such a substantial character of the hydrogen bonds of quinhydrone can couple to an IR-active vibration of the lattice due to electron transfer raises additional questions related to the coupled dynamics of electrons and protons in the materials like quinhydrone. These questions will necessitate further experimentation and theorizing, which is beyond the scope of the present study. Nonetheless these results highlight the complex and rich physics of HBCT materials.

IV. CONCLUSIONS

We have presented experimental, computational and analytical theoretical evidence of a resonant phonon-phonon interaction in the HBCT material quinhydrone similar to the configuration interaction first explained by Fano. However, unlike Fano's treatment we have shown such an interaction between discrete states in the absence of a continuum. DFT calculations of the electronic structure of quinhydrone find two degenerate vibrations delocalized on both the donor and acceptor molecules of this material whose frequency qualitatively match our measurements. Based on the nonlinear Peierls-Hubbard

Hamiltonian, we believe the mechanism leading to this phonon-phonon interaction is the first *and* second order corrections to the adiabatic wave functions of quinhydrone due to electron-phonon coupling. This behavior of quinhydrone shows that spontaneous fluctuations in the localization of electron density on different molecular sites can lead to a complex interaction between discrete vibrational eigenstates of its crystalline lattice, which to our knowledge has yet to be observed in any other material. First principles modeling of the Raman scattering process using time-dependent perturbation theory finds that this mechanism can provide excellent qualitative agreement with our measurements excited in the visible region. This modeling shows that the deviation of the harmonic frequency of each vibration stems from interference between the quantum mechanical pathways taking part in the inelastic light scattering process, as one would expect from a Fano-like resonant interaction.

Interference between discrete resonances has been observed previously in nano-structures⁵⁴, plasmonic structures⁵⁵ as well as metamaterials composed of plasmonic unit cells⁵⁶. However, to our knowledge the coherent coupling of discrete phonons forming a Fano-like res-

onant interaction has thus far been unobserved in a bulk material, either organic or inorganic, driven by any kind of mechanism. In addition, based on isotopic substitution these results may be driven by electron-proton interactions native to hydrogen-bonded charge-transfer materials. These results may shed light on the discrepancy between recent theoretical assessments of the ability of organic HBCT materials to attain room temperature ferroelectric phases, expand the physical mechanisms that produce phonon-phonon interactions and demonstrate the rich physical phenomena present in hydrogen-bonded materials that may lead to their further application in electronics and photonics.

Appendix A: Nonlinear Electron Transfer Polaron Wavefunctions

Following the line of reasoning detailed in Section II.C. and standard time-independent perturbation theory, the unnormalized electron transfer polaron wave functions pertinent to 2.33 eV excitation in the presence of both linear and nonlinear electron-phonon coupling become,

$$|\Psi_1\rangle = |\Psi_A\rangle|0\rangle_j|0\rangle_l + |\Psi_B\rangle \left\{ 2a_1a_2\sqrt{2} \left[\frac{\langle\Psi_B|g_j|\Psi_A\rangle}{E_{A,00} - E_{B,10}}|1\rangle_j|0\rangle_l + \frac{\langle\Psi_B|g_l|\Psi_A\rangle}{E_{A,00} - E_{B,01}}|0\rangle_j|1\rangle_l \right] \right. \\ \left. + 8|a_1a_2|^2 \left[\left(\frac{|\langle\Psi_B|G_{jj}^{(1)}|\Psi_A\rangle|^2 + |\langle\Psi_B|G_{ll}^{(1)}|\Psi_A\rangle|^2}{E_{A,00} - E_{B,00}} \right) |0\rangle_j|0\rangle_l + \frac{|\langle\Psi_B|G_{jl}^{(1)}|\Psi_A\rangle|^2}{E_{A,00} - E_{B,11}}|1\rangle_j|1\rangle_l \right] \right\}, \quad (\text{A1a})$$

$$|\Psi_2\rangle = |\Psi_A\rangle|1\rangle_j|0\rangle_l + |\Psi_B\rangle \left\{ 2a_1a_2\sqrt{2} \left[\frac{\langle\Psi_B|g_j|\Psi_A\rangle}{E_{A,10} - E_{B,20}}|2\rangle_j|0\rangle_l + \frac{\langle\Psi_B|g_l|\Psi_A\rangle}{E_{A,10} - E_{B,01}}|1\rangle_j|1\rangle_l \right] \right. \\ \left. + \frac{\langle\Psi_B|g_j^*|\Psi_A\rangle}{E_{A,10} - E_{B,00}}|0\rangle_j|0\rangle_l \right] + 8|a_1a_2|^2 \left[\frac{|\langle\Psi_B|G_{jl}^{(2)}|\Psi_A\rangle|^2}{E_{A,10} - E_{B,21}}|2\rangle_j|1\rangle_l + \frac{|\langle\Psi_B|G_{jl}^{(3)}|\Psi_A\rangle|^2}{E_{A,00} - E_{B,01}}|0\rangle_j|1\rangle_l \right] \right\}, \quad (\text{A1b})$$

$$|\Psi_3\rangle = |\Psi_B\rangle|0\rangle_j|0\rangle_l - |\Psi_A\rangle \left\{ 2a_1a_2\sqrt{2} \left[\frac{\langle\Psi_A|g_j|\Psi_B\rangle}{E_{B,00} - E_{A,10}}|1\rangle_j|0\rangle_l + \frac{\langle\Psi_A|g_l|\Psi_B\rangle}{E_{B,00} - E_{A,01}}|0\rangle_j|1\rangle_l \right] \right. \\ \left. - 8|a_1a_2|^2 \left[\left(\frac{|\langle\Psi_A|G_{jj}^{(1)}|\Psi_B\rangle|^2 + |\langle\Psi_A|G_{ll}^{(1)}|\Psi_B\rangle|^2}{E_{A,00} - E_{B,00}} \right) |0\rangle_j|0\rangle_l + \frac{|\langle\Psi_A|G_{jl}^{(1)}|\Psi_B\rangle|^2}{E_{B,00} - E_{A,11}}|1\rangle_j|1\rangle_l \right] \right\}, \quad (\text{A1c})$$

$$|\Psi_4\rangle = |\Psi_B\rangle|1\rangle_j|0\rangle_l - |\Psi_A\rangle \left\{ 2a_1a_2\sqrt{2} \left[\frac{\langle\Psi_A|g_j|\Psi_B\rangle}{E_{B,10} - E_{A,20}}|2\rangle_j|0\rangle_l + \frac{\langle\Psi_A|g_l|\Psi_B\rangle}{E_{B,10} - E_{A,01}}|1\rangle_j|1\rangle_l \right] \right. \\ \left. + \frac{\langle\Psi_A|g_j^*|\Psi_B\rangle}{E_{B,10} - E_{A,00}}|0\rangle_j|0\rangle_l \right] - 8|a_1a_2|^2 \left[\frac{|\langle\Psi_A|G_{jl}^{(2)}|\Psi_B\rangle|^2}{E_{B,10} - E_{A,21}}|2\rangle_j|1\rangle_l + \frac{|\langle\Psi_A|G_{jl}^{(3)}|\Psi_B\rangle|^2}{E_{B,00} - E_{A,01}}|0\rangle_j|1\rangle_l \right] \right\}. \quad (\text{A1d})$$

for the j^{th} phonon mode.

Appendix B: Calculations of Raman Scattering Cross-Section in the Presence of Nonlinear Electron-Phonon Coupling

The wave functions of Eq. (A1) define the single electron polaron states of quinhydrone due to linear and non-

linear e-ph coupling for the case of 2.33 eV excitation. To calculate Raman spectra, we also introduce quantized electromagnetic fields at the laser and Stokes scattered frequencies, ω_L and ω_S , respectively. For the time perturbative theoretical treatment of resonant spontaneous light scattering, as is the case in our experiments excited

at both 1.58 eV and 2.33 eV, we only take matrix elements of the form $\langle \Psi_i | \bar{\mathbf{A}} \cdot \bar{\mathbf{p}} | \Psi_n \rangle \langle \Psi_n | \bar{\mathbf{A}} \cdot \bar{\mathbf{p}} | \Psi_f \rangle$ to account for the perturbation to the momentum of the material's electrons, $\bar{\mathbf{p}}$, in the presence of a quantized electromagnetic vector potential $\bar{\mathbf{A}}$ ^{57,58}. Considering the correct creation and annihilation of photons, Eq. (A1) shows

that the states of the scattering process correspond to

$$|\Psi_i\rangle = |\Psi_1\rangle|0\rangle_S|N\rangle_L, \quad (\text{B1a})$$

$$|\Psi_n^{(1)}\rangle = |\Psi_3\rangle|0\rangle_S|N-1\rangle_L, \quad (\text{B1b})$$

$$|\Psi_n^{(2)}\rangle = |\Psi_4\rangle|0\rangle_S|N-1\rangle_L, \quad (\text{B1c})$$

$$|\Psi_f\rangle = |\Psi_2\rangle|1\rangle_S|N-1\rangle_L. \quad (\text{B1d})$$

where one must sum over the intermediate states $|\Psi_n^{(1)}\rangle$ and $|\Psi_n^{(2)}\rangle$ to correctly calculate the spectra. Inspecting the explicit form of the polaron wave functions, we see that in order to excite fundamentals of either the j^{th} or l^{th} mode, only two sets of matrix elements significantly contribute to the scattering process. Explicitly, these matrix elements of interest become,

$$\begin{aligned} \langle \Psi_i | \bar{\mathbf{A}} \cdot \bar{\mathbf{p}} | \Psi_n \rangle \langle \Psi_n | \bar{\mathbf{A}} \cdot \bar{\mathbf{p}} | \Psi_f \rangle = & \quad (\text{B2}) \\ s \langle 0|_L \langle N| \langle \Psi_A | \bar{\mathbf{A}}_L \cdot \bar{\mathbf{p}} | \Psi_B \rangle |N-1\rangle_L |0\rangle_{SS} \langle 0|_L \langle N-1| \langle \Psi_B | \bar{\mathbf{A}}_S \cdot \bar{\mathbf{p}} | \Psi_A \rangle |N-1\rangle_L |1\rangle_S \\ \times [A_j |\langle 0|_l \langle 0|_j \langle 1|1\rangle_j + A_l |\langle 0|_l \langle 0|_j \langle 1|1\rangle_l], \end{aligned}$$

where,

$$A_j = -\frac{16|a_1 a_2|^2 a_1 a_2 \sqrt{2}}{\mathcal{N}_1 \mathcal{N}_2 \mathcal{N}_4^2} \frac{\langle \Psi_A | g_j^* | \Psi_B \rangle}{E_{B,10} - E_{A,00}} \left(\frac{|\langle \Psi_B | G_{jj}^{(1)} | \Psi_A \rangle|^2 + |\langle \Psi_B | G_{ll}^{(1)} | \Psi_A \rangle|^2}{E_{A,00} - E_{B,00}} \right), \quad (\text{B3a})$$

$$A_l = -\frac{16|a_1 a_2|^2 a_1 a_2 \sqrt{2}}{\mathcal{N}_1 \mathcal{N}_2 \mathcal{N}_3^2} \frac{\langle \Psi_A | g_l | \Psi_B \rangle}{E_{B,00} - E_{A,01}} \frac{|\langle \Psi_B | G_{jl}^{(3)} | \Psi_A \rangle|^2}{E_{A,00} - E_{B,01}}, \quad (\text{B3b})$$

and the factor \mathcal{N}_i corresponds to the normalization constant for the i^{th} polaron state of Eq. (A1). All other terms that lead to fundamental excitations of either the j^{th} or l^{th} mode possess at least two more factors of the perturbative coupling constants, making their contribution to the overall scattering process significantly smaller than the terms shown in Eq. (12). Thus, from standard time-dependent perturbation theory the second order correction that leads to scattering transitions in the presence of the linear and nonlinear electron-phonon interactions becomes proportional to

$$\begin{aligned} c^{(2)}(t) \propto \frac{|\mu_{AB}|^2}{\hbar} \left[\frac{A_j}{\omega_{14} - \omega_L + i\Gamma_j} \int_0^t \exp(-\hbar\Gamma_j t') \exp(i\hbar\{\omega_S + \omega_j - \omega_L\}t') dt' \right. \\ \left. + \frac{A_l}{\omega_{13} - \omega_L + i\Gamma_l} \int_0^t \exp(-\hbar\Gamma_l t') \exp(i\hbar\{\omega_S + \omega_l - \omega_L\}t') dt' \right], \quad (\text{B4}) \end{aligned}$$

where ω_j and ω_l are the angular frequencies and Γ_j and Γ_l are the phenomenological dephasing rates of the j^{th} and l^{th} modes, respectively, while $\hbar\omega_{13} = E_1 - E_3$ and $\hbar\omega_{14} = E_1 - E_4$. For Eq. (B4), we have also used the relation $|\langle 0|_l \langle 0|_j \langle 1|1\rangle_j = |\langle 0|_j \langle 0|_l \langle 1|1\rangle_l = 1$, as would be expected of harmonic oscillator eigenstates and have accounted for the appropriate creation and annihilation of excitations of the fields at the laser and Stokes frequencies as dictated by Eq. (B2). $\mu_{AB} = \langle B | \mu | A \rangle$ is the electronic transition dipole moment found by applying the uncertainty principle between the position and momentum of the electronic state coupled to the incident and scattered fields. The scattering transition rate is proportional to $|c^{(2)}(t)|^2$, which, as $t \rightarrow \infty$, becomes,

$$\begin{aligned} |c^{(2)}(t)|^2 = c^{(2)}(t) c^{*(2)}(t) \propto \frac{|\mu_{AB}|^4}{\hbar^2} \left[\frac{|A_{jj}|^2}{\{\omega_j - \omega\}^2 + \Gamma_j^2} + \frac{|A_{ll}|^2}{\{\omega_l - \omega\}^2 + \Gamma_l^2} \right. \\ \left. + \frac{A_{jj} A_{ll}^*}{\{\omega_j - \omega\} \{\omega_l - \omega\} + \Gamma_j \Gamma_l} + \frac{A_{jj}^* A_{ll}}{\{\omega_j - \omega\} \{\omega_l - \omega\} + \Gamma_j \Gamma_l} \right], \quad (\text{B5}) \end{aligned}$$

where $A_{jj} = A_j/\omega_{14} - \omega_L + i\Gamma_j$, $A_{ll} = A_l/\omega_{13} - \omega_L + i\Gamma_l$ and $\omega = \omega_L - \omega_S$ allows one to calculate a spectrum as a function of frequency.

ACKNOWLEDGMENTS

The author thanks Prof. Jahan Dawlaty for the support to study the spectroscopic properties of quinhydrone

single crystals, providing resources for experimental and computational work, and securing the financial support necessary through the University of Southern California start up grant, the AFOSR YIP Award (FA9550-13-1-0128) and the Rose Hills Foundation Research Fellowship. In addition, the author thanks Dr. Evgeniia Butaeva for useful feedback on the manuscript and Dr. Frank Devlin for technical assistance with the Raman spectrometer.

* arury@usc.edu

- ¹ R. E. Peierls, *Quantum Theory of Solids* (Oxford University Press, New York, 2001).
- ² C. Kittel, *Introduction to Solid State Physics* (John Wiley & Sons, New York, 2004).
- ³ B. Fultz, *Progress in Materials Science* **55**, 247 (2010).
- ⁴ J. F. Scott, *Physical Review Letters* **21**, 907 (1968).
- ⁵ D. L. Rousseau and S. P. S. Porto, *Physical Review Letters* **20**, 1354 (1968).
- ⁶ J. Menéndez and M. Cardona, *Physical Review B* **29**, 2051 (1984).
- ⁷ R. Cuscó, E. Alarcón-Lladó, J. Ibáñez, L. Artús, J. Jiménez, B. Wang, and M. J. Callahan, *Physical Review B* **75**, 165202 (2007).
- ⁸ N. Bonini, M. Lazzeri, N. Marzari, and F. Mauri, *Physical Review Letters* **99**, 176802 (2007).
- ⁹ E. J. Heller, *Accounts of Chemical Research* **14**, 368 (1981).
- ¹⁰ R. A. Cowley, *Reports on Progress in Physics* **31**, 123 (1968).
- ¹¹ J. S. Brooks, *Chemical Society Review* **39**, 2667 (2010).
- ¹² A. S. Tayi, A. K. Shveyd, A. C.-H. Sue, J. M. Szarko, B. S. Rolczynski, D. Cao, T. J. Kennedy, A. A. Sarjeant, C. L. Stern, W. F. Paxton, W. Wu, S. K. Dey, A. C. Fahrenbach, J. R. Guest, H. Mohseni, L. X. Chen, K. L. Wang, J. F. Stoddart, and S. I. Stupp, *Nature* **488**, 485 (2012).
- ¹³ A. Ueda, S. Yamada, T. Isono, H. Kamo, A. Nakao, R. Kumai, H. Nakao, Y. Murakami, K. Yamamoto, Y. Nishio, and H. Mori, *Journal of the American Chemical Society* **136** (2014).
- ¹⁴ G. P. Stahly, *Crystal Growth & Design* **9**, 4212 (2009).
- ¹⁵ T. Sakurai, *Acta Crystallographica Section B Structural Crystallography and Crystal Chemistry* **24**, 403 (1968).
- ¹⁶ T. Mitani, G. Saito, and H. Urayama, *Physical Review Letters* **60**, 2299 (1988).
- ¹⁷ A. S. Rury, S. Sorenson, E. Driscoll, and J. M. Dawlaty, *The Journal of Physical Chemistry Letters* **6**, 3560 (2015).
- ¹⁸ G. D'Avino and M. J. Verstraete, *Physical Review Letters* **113**, 237602 (2014).
- ¹⁹ H. Okamoto, Y. Ishige, S. Tanaka, H. Kishida, S. Iwai, and Y. Tokura, *Physical Review B* **70**, 1 (2004).
- ²⁰ S. Horiuchi, Y. Okimoto, R. Kumai, and Y. Tokura, *Science* **299**, 229 (2003).
- ²¹ L. Del Freo, A. Painelli, and Z. G. Soos, *Physical Review Letters* **89**, 027402 (2002).
- ²² H. Uemura and H. Okamoto, *Physical Review Letters* **105**, 1 (2010).
- ²³ L. Cavatorta, A. Painelli, and Z. G. Soos, *Physical Review B* **91**, 174301 (2015).
- ²⁴ T. Yildirim, O. Gülseren, J. W. Lynn, C. M. Brown, T. J. Udovic, Q. Huang, N. Rogado, K. A. Regan, M. A. Hayward, J. S. Slusky, T. He, M. K. Haas, P. Khalifah, K. Inumaru, and R. J. Cava, *Physical Review Letters* **87**, 037001 (2001).
- ²⁵ B. Renker, K. B. Bohnen, R. Heid, D. Ernst, H. Schober, M. Koza, P. Adelman, P. Schweiss, and T. Wolf, *Physical Review Letters* **88**, 067001 (2002).
- ²⁶ A. Shukla, M. Calandra, M. d'Astuto, M. Lazzeri, F. Mauri, C. Bellin, M. Krisch, J. Karpinski, S. M. Kazakov, J. Jun, D. Daghero, and K. Parlinski, *Physical Review Letters* **90**, 095506 (2003).
- ²⁷ E. Cappelluti, *Physical Review B* **73**, 140505 (2006).
- ²⁸ P. P. Singh, *Physical Review Letters* **97**, 247002 (2006).
- ²⁹ A. Mialitsin, B. S. Dennis, N. D. Zhigadlo, J. Karpinski, and G. Blumberg, *Physical Review B* **75**, 020509 (2007).
- ³⁰ R. Bozio, A. Feis, I. Zanon, and C. Pecile, *The Journal of Chemical Physics* **91**, 13 (1989).
- ³¹ D. Pedron, A. Speghini, V. Mulloni, and R. Bozio, *The Journal of Chemical Physics* **103**, 2795 (1995).
- ³² A. S. Rury, S. Sorenson, and J. M. Dawlaty, *The Journal of Chemical Physics* **144**, 104701 (2016).
- ³³ T. C. Damen, S. P. S. Porto, and B. Tell, *Physical Review* **142**, 570 (1966).
- ³⁴ U. Fano, *Physical Review* **124**, 1866 (1961).
- ³⁵ S. Naler, M. Rübhausen, S. Yoon, S. L. Cooper, K. H. Kim, and S. W. Cheong, *Physical Review B* **65**, 092401 (2002).
- ³⁶ H. Rho, S. L. Cooper, S. Nakatsuji, H. Fukazawa, and Y. Maeno, *Physical Review B* **68**, 100404 (2003).
- ³⁷ W. Borer, S. Mitra, and K. Namjoshi, *Solid State Communications* **9**, 1377 (1971).
- ³⁸ A. D. Becke, *Physical Review A* **38**, 3098 (1988).
- ³⁹ J. P. Perdew, in *Electronic Structure of Solids 1991*, Vol. 11, edited by P. Ziesche and E. Eschrig (Akademie Verlag, 1991) pp. 11–20.
- ⁴⁰ C. Gatti, V. R. Saunders, and C. Roetti, *The Journal of Chemical Physics* **101**, 10686 (1994).
- ⁴¹ R. Dovesi, M. Causà, R. Orlando, C. Roetti, and V. R. Saunders, *The Journal of Chemical Physics* **92**, 7402 (1990).
- ⁴² R. Dovesi, R. Orlando, A. Erba, C. M. Zicovich-Wilson, B. Civalleri, S. Casassa, L. Maschio, M. Ferrabone, M. D. L. Pierre, P. D'Arco, Y. Noël, M. Causà, M. Rérat, and B. Kirtman, *Int. J. Quantum Chem.* **114**, 1287 (2014).
- ⁴³ F. Pascale, C. M. Zicovich-Wilson, F. López Gejo, B. Civalleri, R. Orlando, and R. Dovesi, *Journal of Computational Chemistry* **25**, 888 (2004).
- ⁴⁴ C. M. Zicovich-Wilson, F. Pascale, C. Roetti, V. R. Saunders, R. Orlando, and R. Dovesi, *Journal of Computational Chemistry* **25**, 1873 (2004).

- ⁴⁵ R. M. Hanson, *Journal of Applied Crystallography* **43**, 1250 (2010).
- ⁴⁶ A. Painelli and A. Girlando, *The Journal of Chemical Physics* **84**, 5655 (1986).
- ⁴⁷ V. Coropceanu, R. S. Sánchez-Carrera, P. Paramonov, G. M. Day, and J.-L. Brédas, *The Journal of Physical Chemistry C* **113**, 4679 (2009).
- ⁴⁸ A. Girlando, R. Bozio, C. Pecile, and J. B. Torrance, *Physical Review B* **26**, 2306 (1982).
- ⁴⁹ M. J. G. Moa, M. Mandado, and R. A. Mosquera, *Journal of Physical Chemistry A* **111**, 1998 (2007).
- ⁵⁰ H. Trommsdorff, *Chemical Physics Letters* **1**, 214 (1967).
- ⁵¹ R. Pou-Amerigo, M. Merchan, and E. Orti, *The Journal of Chemical Physics* **110**, 9536 (1999).
- ⁵² A. S. Rury, *Physical Review A* **87**, 043408 (2013).
- ⁵³ J. G. Skinner and W. G. Nilsen, *Journal of the Optical Society of America* **58**, 113 (1968).
- ⁵⁴ A. E. Miroshnichenko, S. Flach, and Y. S. Kivshar, *Review of Modern Physics* **82**, 2257 (2010).
- ⁵⁵ A. S. Rury, *Physical Review B* **88**, 205132 (2013).
- ⁵⁶ B. Luk'yanchuk, N. I. Zheludev, S. A. Maier, N. J. Halas, P. Nordlander, H. Giessen, and C. T. Chong, *Nature Materials* **9**, 707 (2010).
- ⁵⁷ J. Sakurai, *Advanced Quantum Mechanics* (Addison-Wesley, Reading, MA, 1967).
- ⁵⁸ M. Cardona, in *Light Scattering in Solids II: Basic Concepts and Instrumentation*, Topics in Applied Physics, edited by M. Cardona and G. Güntherodt (Springer-Verlag, Berlin, 1982) Chap. 2.